Supporting Information

Polycation-regulated hydrogel electrolytes with nanoscaled hydrophobic confinement inducing Zn (002) deposition for highly reversible zinc anodes

Xilin Wang,[a,b] Bin Wang,*[b] Pengyang Lei,[a] Xiaorui Wang,[a] Lei Zhou,[b] Junxiang Zhang,[b] Jinyang Zhang [b] and Jianli Cheng*[a]

Experimental Section

Materials

The chemicals were received without further purification: dimethyl aminopropyl methacrylamide (DMAPMA, AR, 99%), 1-bromooctadecane (C_{18}-Br, AR, 98%), acetone (AR, 99%), diethyl ether (AR, 99%), 2-hydroxy-4'-(2-hydroxyethoxy)-2-methylpropiophenone (AR, 98%), acrylamide (AAm, AR, 99%), zinc sulfate heptahydrate ($ZnSO_4$•$7H_2O$, AR, 99%), manganese sulfate monohydrate ($MnSO_4$•H_2O, AR, 99%), manganous acetate tetrahydrate ($C_4H_{14}MnO_8$, AR, 98%), potassium permanganate ($KMnO_4$, AR, 99%), multi-walled carbon nanotubes (C-MWCNTs, length < 10 μm, 30-50 nm).

1.2 Preparation of DMAPMA-C_{18} monomer

Typically, DMAPMA (8.51 g) and 1-bromooctadecane (C_{18}-Br) (20.0 g) were added into 40 mL anhydrous acetone and mechanically stirred under 55 °C under nitrogen protection. After 48 h, rotary evaporation was employed to remove the acetone. Then, diethyl ether (50 mL) was added and the sediments were washed three times by filtration with diethyl ether and then put into the vacuum chamber overnight to obtain the final product.

1.3 Preparation of C_{18}-PCHA-AAm hydrogel electrolytes

Typically, DMAPMA-C_{18} (0.3 g) and AAm (0.7 g) were added into 4 ml deionized water and were stirred for 30 min. Then, 2-hydroxy-4'-(2-hydroxyethoxy)-2-methylpropiophenone (0.01 g) were added into the above solution to perform the polymerization reaction by UV light (365 nm) for 15 min. The PAAm hydrogels (AAm, 1.0 g) were obtained under the same reaction conditions without DMAPMA-C_{18}. These obtained hydrogels were soaked into 2 M $ZnSO_4$ (1000 ml) solution to obtain the hydrogel electrolytes under the same soaking time.

1.4 Preparation of electrodes

The MnO_2/C-MWCNTs composite was synthesized by a hydrothermal method. In a typical synthesis run, C-MWCNTs (0.3 g) were dispersed into deionized water (150 ml). Then, $Mn(CH_3COO)_2 \cdot 4H_2O$ (2.94 g) were added into the above solution under continuous stirring for 0.5 h. Subsequently, the mixed solution was added dropwise into the 80 ml solution containing $KMnO_4$ (1.27 g) and stirred for 0.5 h. The mixed solution was treated by ultrasonic dispersion for 10 min and transferred to a teflon-

lined autoclave and heated at 120 ℃ for 12 h. Finally, the product was washed several times with deionized water and dried at 80 ℃ in a vacuum oven for 8 h to obtain the MnO_2/C-MWCNTs composite. The cathodes were obtained by casting the slurry of MnO_2/C-MWCNTs composite, acetylene black, carboxymethylcellulose (CMC), styrene-butadiene rubber (SBR) and at a weight ratio of 70:20:7:3 on the surface of Ti foil. Then the cathode was dried at 60 ℃ in a vacuum oven for 8 h to finally obtain the MnO_2 cathode. The effective mass loading of MnO_2 is 0.5~1.5 mg cm^{-2}. Typically, DMAPMA-C_{18} (0.3 g) and AAm (0.7 g) were added into 4 ml deionized water and were stirred for 30 min. Then, 2-hydroxy-4'-(2-hydroxyethoxy)-2-methylpropiophenone (0.01 g) which acted as initiators were added into the above solution. The solution was dropped onto Zn foils in home-made molds with controllable thickness to perform the polymerization reaction by UV light (365 nm) for 15 min. The obtained Zn-hydrogel composites were soaked into 2 M $ZnSO_4$ and 0.1 M $MnSO_4$ (1000 ml) solution to obtain Zn/hydrogel electrolyte composites. Finally, two separated C_{18}-PCHA-AAm/Zn foil were integrated through healing ability.

1.5 Fabrication of flexible AZIBs

Flexible AZIBs were assembled by sandwiching the hydrogel electrolyte/Zn foil and the cathode together, which was reinforced and protected by using an aluminum plastic film.

1.6 Characterizations

Nuclear magnetic resonance (NMR) measurements were performed on a 500 MHz NMR spectrometer. X-ray diffraction (XRD) profiles were performed using a D2 Phaser diffractometer at 25 °C. A Fourier transform infrared spectrometer (FTIR, WQF-530F120) was used to characterize hydrogel electrolytes. The tensile test and lap-shear test were performed on a universal tensile testing machine. The galvanostatic charge and discharge test was carried out by using the LANHE CT2001A testing system. Electrochemical impedance spectroscopy (EIS), linear scanning voltammetry (LSV), and cyclic voltammetry (CV) were conducted using an electrochemical workstation. The surface morphology and energy disperse spectroscopy (EDS) were characterized by a scanning electron microscope (SEM, Hitachi Regulus8100). The contact angle was characterized by a contact angle measurement system (SDC-80). Confocal laser scanning microscopy (LEXT-OLS5000) was used to study the Zn foil surface. The Zeta potentials were collected using Malvern Zetasizer Nano ZS90.

1.7 Electrochemical measurement

The ionic conductivity σ (mS cm^{-1}) of the electrolytes was measured using EIS (0.1 Hz to 10 k Hz). A piece of the prepared hydrogel electrolyte was placed between two stainless sheets. The conductivity σ was calculated according to the following formula:

$$\sigma = \frac{L}{R \times A} \qquad (1)$$

, where L (cm), A (cm^2), and R (Ω) are the thickness, electrode contact area, and bulk resistance. The Zn ion transference number was obtained according to the typical Evans method, which should be described as the following formula:

$$t_{Zn^{2+}} = \frac{I_S(\Delta V - I_0 R_0)}{I_0(\Delta V - I_S R_S)} \qquad (2)$$

, where ΔV (10 mV) is the constant polarization potential. LSV measurements were carried out using Ti foil as working electrode and a Zn plate as reference and counter electrodes. CV curves of Zn plating/stripping were measured where Ti was used as working electrode and the Zn plates as reference and counter electrodes. Galvanostatic charge-discharge (GCD) measurements were performed using a LANHE CT2001A battery-test system. Symmetric cells were assembled to assess the stability of the hydrogel electrolytes. In symmetric Zn//Zn cells, two identical bare Zn plates, with a diameter of 12 mm, were used as negative and positive electrodes. EIS plots of Zn-MnO_2 batteries were carried out from 1 MHz to 0.01 Hz. The Zn_{DOD} was obtained according to the following formula:

$$Zn_{DOD} = \frac{C \times S}{m \times 820\ mAh\ g^{-1}} \qquad (3)$$

, where C (mAh cm^{-2}) is the testing specific capacity, S (cm^2) is the Zn foil's area, m (g) is the weight of the Zn foil.

1.8 Calculation Details

Hydrogel electrolytes with a polymerization degree of 5 was used to simulate the adsorption behavior of the long polymer chain with the Zn^{2+}. The geometry optimization and density functional theory (DFT) chemical description for the molecular structures of C_{18}-PCHA-AAm and PAAm compounds were performed using Gaussian 09 program, and B3LYP/6-31G(d,p) basis set (for C, N, O and H atoms) and lanl2dz were used to geometry optimization. All calculations were carried out with the atom-pairwise dispersion correction (DFT-D3) and the implicit universal solvation model based on Solute Electron Density (SMD). The Electrostatic potential (ESP) was analyzed by the Multiwfn package[1] and drawn by VMD package.[2] The conversion formula is as follows:

$$E = E_{a-b} - E_a - E_b \qquad (4)$$

Where E_{a-b} is the total energy after binding, E_a and E_b are the energies of zinc ion and optimized molecule respectively.

The 002 and 101 crystal planes of Zn were extracted from the database and expanded to an appropriate size. The DFT calculation was performed with the GGA/PBE functional and all electrons were treated as valence with a cut off energy of 550 eV. The model of (002) and (101) planes of $4 \times 4 \times 1$ supercell was sliced and an extra vacuum zone of 12 Å was applied along z-direction. Hydrogel electrolytes with an appropriate skeleton was used to simulate the adsorption behavior on Zn surface. The convergence criterion for the electronic self-consistent field (SCF) loop was set to 1×10^{-5} eV per atom. The atomic structures were optimized until the residual forces were below 0.02 eV $Å^{-1}$. The conversion formula is as follows:

$$E = E_{a-b} - E_a - E_b \qquad (5)$$

Where E_{a-b} is the total energy after adsorption, E_a and E_b are the energies of Zn 002/101 surface and optimized molecule respectively.

2. Supporting Figures and Tables

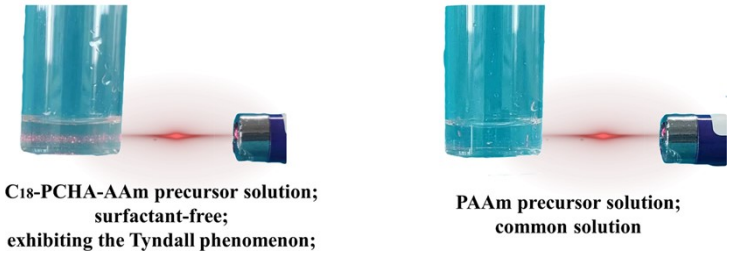

Fig. S1 Illustration of Tyndall phenomenon in C_{18}-PCHA-AAm and PAAm precursor solutions.

As shown in Fig. S1, the cationic water-soluble hydrophobic monomer DMAPMA-C_{18} can serve as a type of surfactant owing to its unique structure, leading to the Tyndall phenomenon. On the contrary, this phenomenon doesn't exist in the common acrylamide solution.

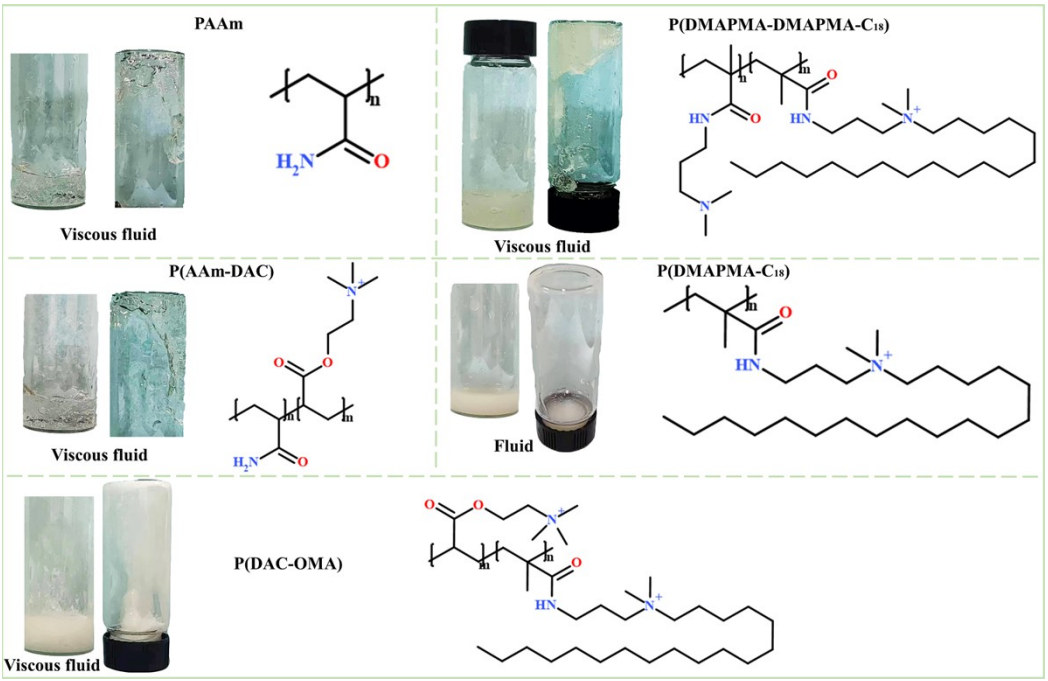

Fig. S2 Illustration of copolymerization products of different monomers.

Table S1 copolymerization of different monomers and corresponding products' properties.

	Monomer 1	Monomer 2	Water (mL)	UV curing	Products' property
PAAm	Acrylamide, 1 g	/	4	15 min	Viscous fluid
P(AAm-DAC)	Acrylamide, 0.7 g	Acryloyloxyethyltrimethyl ammonium chloride (DAC), 0.3 g	4	15 min	Viscous fluid
P(DMAPMA-DMAPMA-C18)	Dimethyl aminopropyl methacrylamide (DMAPMA), 0.7 g	DMAPMA-C18, 0.3 g	4	15 min	Viscous fluid
P(DMAPMA-C18)	DMAPMA-C_{18}, 1 g	/	4	15 min	Fluid
P(DAC-OMA)	DAC, 0.7 g	Octadecyl methacrylate (OMA), 0.3 g	4	15 min	Viscous fluid
This work	Acrylamide, 0.7 g	DMAPMA-C18, 0.3 g	4	15 min	Tough hydrogel

As shown in Table S1 and Fig. S2, the results of PAAm and P(AAm-DAC) demonstrate that a tough and stable hydrogel can't be synthesized without crosslinking of hydrophobic associations. Here, DAC is a common cation monomer. Thus, the remarkable characteristics of C_{18}-PCHA-AAm hydrogel electrolytes mainly stem from the unique monomer DMAPMA-C_{18} rather than PAAm. Besides, the P(DMAPMA-DMAPMA-C_{18}) and P(DMAPMA-C_{18}) are only viscous fluids without PAAm because acrylamide is easy to polymerize and form a hydrogel film. Besides, the presentation of P(DAC-OMA) also demonstrates the superiority of DMAPMA-C_{18} monomer.

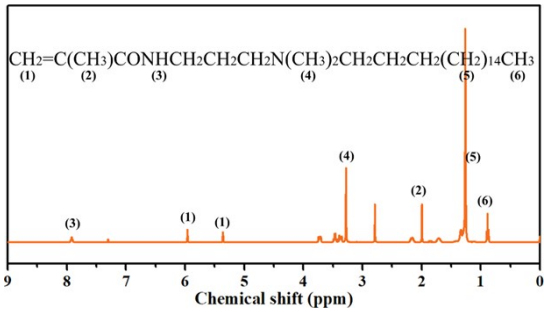

Fig. S3 HNMR spectroscopy of DMAPMA-C_{18}.

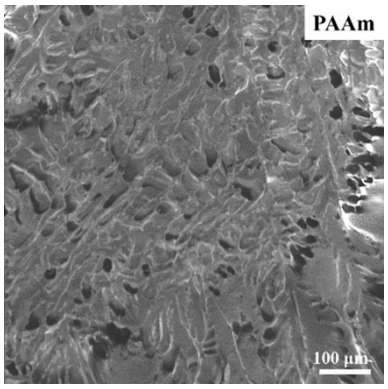

Fig. S4 SEM image of freeze-dried PAAm.

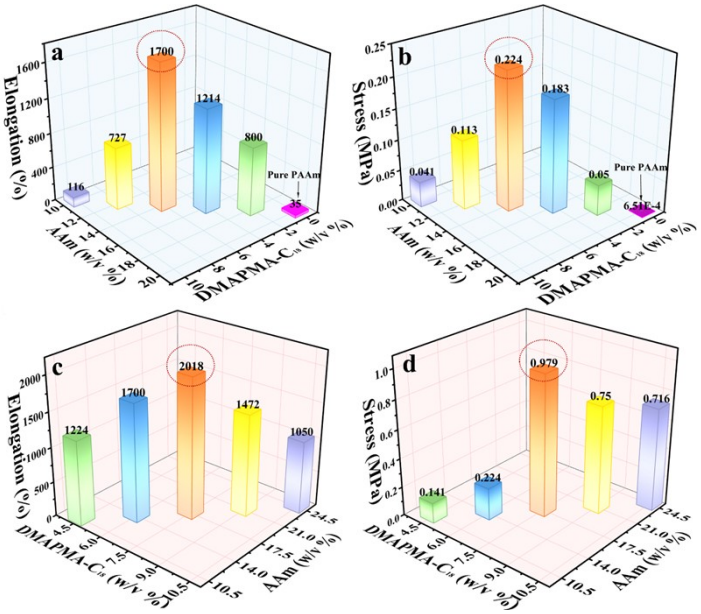

Fig. S5 (a) Ultimate elongation and (b) stress of C_{18}-PCHA-AAm hydrogel with various ratio of DMAPMA-C_{18}/AAm. (c) Ultimate elongation and (d) stress of C_{18}-PCHA-AAm hydrogel with a fixed ratio (DMAPMA-C_{18}/AAm=3/7) and various dosage.

Among the mass ratio of DMAPMA-C_{18}/AAm ranging from 0, 1/9, 2/8, 3/7, 4 /6 to 1, the obtained hydrogel (with the mass ratio of 3/7) exhibits the optimal breaking stress (0.224 MPa) and elongation (1700%). Obviously, the mechanical performances (elongation and stress) first enhance and then decrease with the dosage of DMAPMA-C_{18} increasing. Then, through tuning the ratios of above monomers to water, the obtained hydrogel with 7.5 w/v % DMAPMA-C_{18} and 17.5 w/v % AAm possesses the optimal mechanical properties (elongation: 2018%, stress: 0.979 MPa).

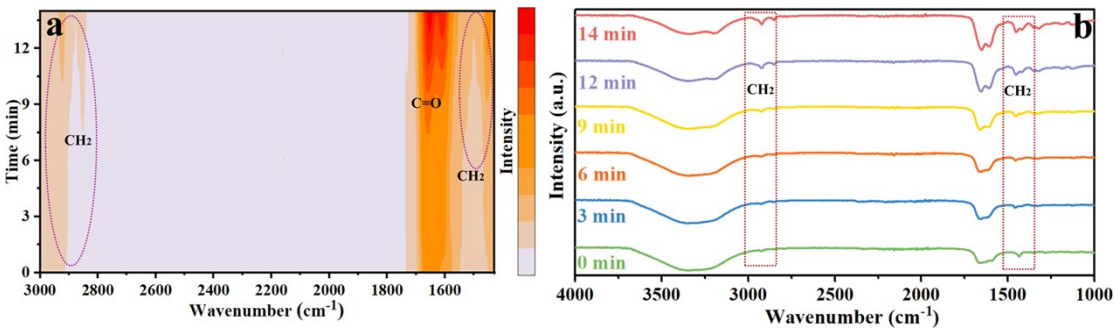

Fig. S6 (a-b) Contour map of the FTIR spectra of in-situ C_{18}-PCHA-AAm on Zn foil in various rection times.

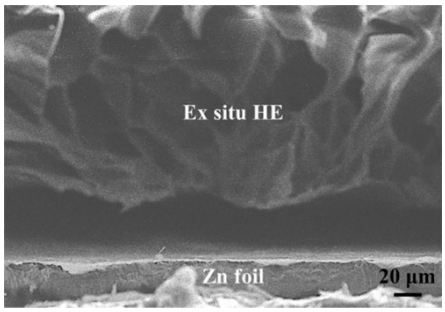

Fig. S7 Sectional SEM image of ex-situ C_{18}-PCHA-AAm/Zn foil.

As depicted in Fig. S7, the ex-situ hydrogel electrolyte has observable gap at the interface. Consequently, Typical hydrogel electrolytes synthesized through ex-situ method tend to generate poor interface, accelerating parasitic reactions and zinc dendrites. On the contrary, in-situ polymerized hydrogel electrolytes can solve the interfacial issues, namely decreased impedance, well-bonded interface and suppression of water activity.

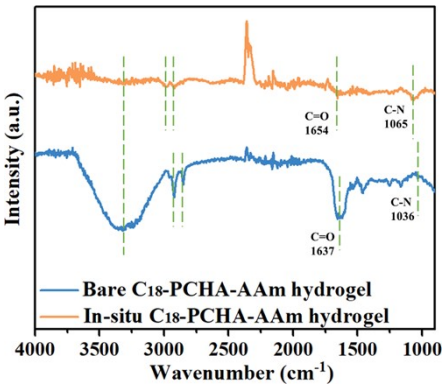

Fig. S8 FTIR spectra of single hydrogel and in-situ hydrogel with Zn foil.

Compared to bare C_{18}-PCHA-AAm hydrogel, the characteristic bands of C=O, C-N are blue-shifted to higher wavenumbers, namely 1654 and 1065 cm^{-2}, respectively, indicating that the complexation of Zn-C_{18}-PCHA-AAm increases the wavenumbers.

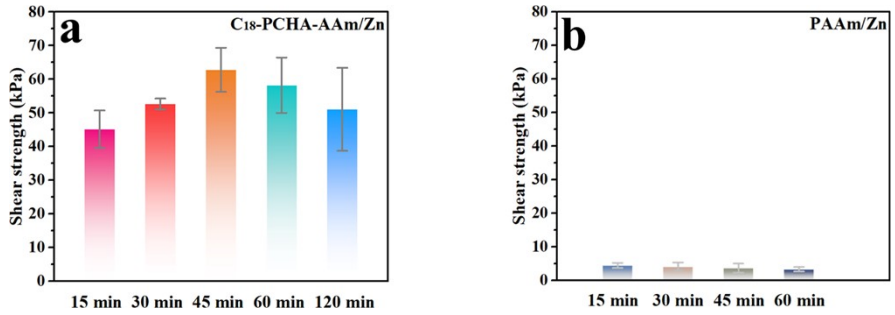

Fig. S9 Zn Shear adhesion strength between in-situ (a) C_{18}-PCHA-AAm and (b) PAAm hydrogel electrolytes and Zn foils with different soaking times.

Surprisingly, the shear adhesion strength between in-situ C_{18}-PCHA-AAm and Zn foils first slowly enhances and then decreases with the extension of soaking time in liquid electrolyte. This strong interfacial adhesion can be attributed to the abundant hydrophobic associations and anti-swelling ability of C_{18}-PCHA-AAm. On the contrary, the PAAm shows limited adhesion and the interfacial adhesion significantly decreases with various soaking times owing to its solubility.

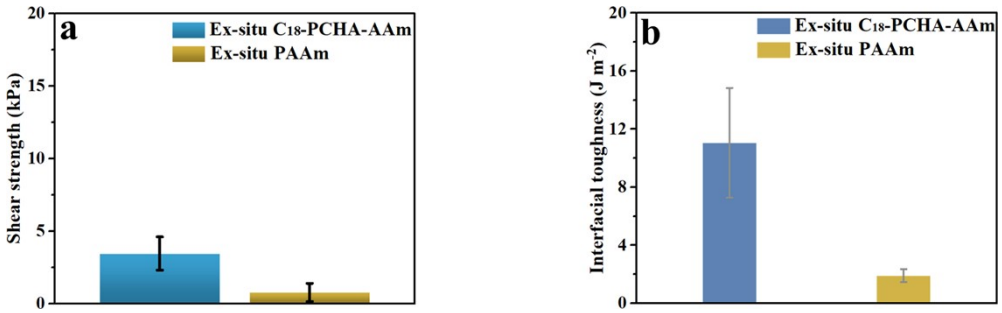

Fig. S10 (a) Zn Shear adhesion strength and (b) interfacial toughness between ex-situ C_{18}-PCHA-AAm, ex-situ PAAm hydrogel electrolytes and Zn foils. The hydrogel electrolyte was pressed onto Zn foil with a slight force for 10 min resting to test.

The ex-situ hydrogel electrolytes both exhibit much lower shear strength and interfacial toughness, indicating that the C_{18}-PCHA-AAm precursor solution may penetrate into Zn surface's pores to increase contact areas and form abundant interactions during the in-situ polymerization, resulting in the compact hydrogel electrolyte/Zn interface.

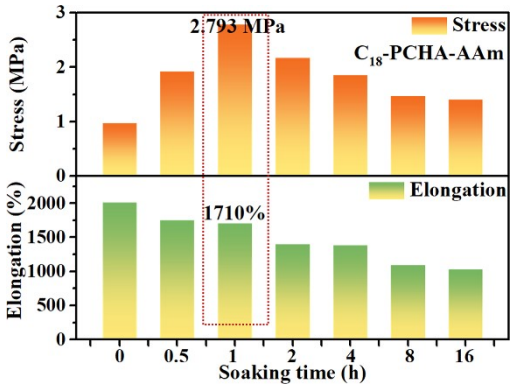

Fig. S11 Ultimate elongation and stress of C_{18}-PCHA-AAm hydrogel soaking in 2 M $ZnSO_4$ for different times.

By tuning the soaking time in large amounts of 2 M $ZnSO_4$ solutions, the optimal C_{18}-PCHA-AAm hydrogel electrolyte can be obtained with remarkable breaking stress (2.793 MPa) and elongation (1710%).

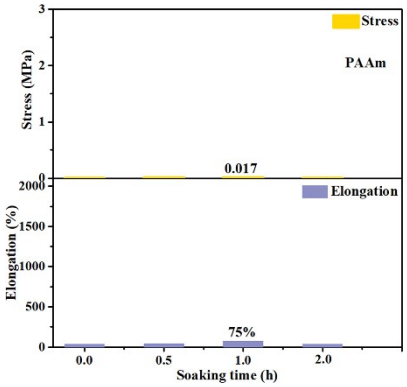

Fig. S12 Ultimate elongation and stress of PAAm hydrogel soaking in 2 M $ZnSO_4$ for different times.

As depicted in Fig. S11, S12, the mechanical properties of PAAm are always inferior to C_{18}-PCHA-AAm despite the various soaking times, indicating that the DMAPMA-C_{18} monomer endows the entire hydrogel electrolyte unique characteristics.

Conventional hydrogels (e.g., PAAm) possess high hydrophilicity and tend to absorb large amounts of water, leading to distinct mechanical and electrochemical deterioration. When hydrophilic hydrogel is soaking into liquid electrolytes, the linear macromolecular chains can be extending and loosely dispersed. On the contrary, the hydrophobic chains in C_{18}-PCHA-AAm can aggregate and expel the water molecules, thus ensuring the structural stability. The multiple hydrophobic associations, acting as crosslinkers, can enhance the crosslink density in hydrogel, further suppressing the swelling ratio.

Consequently, the limited swelling ratio and abundant interactions endow the entire C_{18}-PCHA-AAm hydrogel electrolyte high robustness.

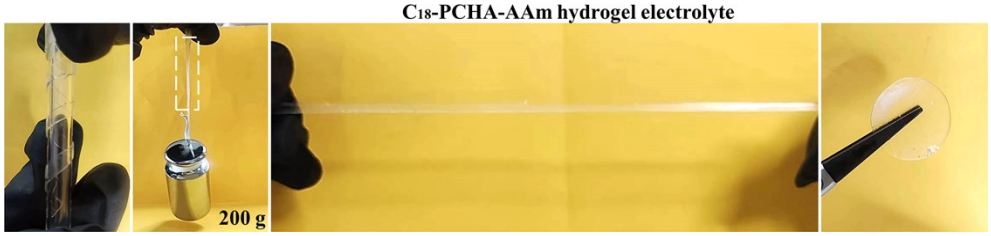

Fig. S13 Photographs of C_{18}-PCHA-AAm hydrogel electrolyte at twisting, holding, and stretching states.

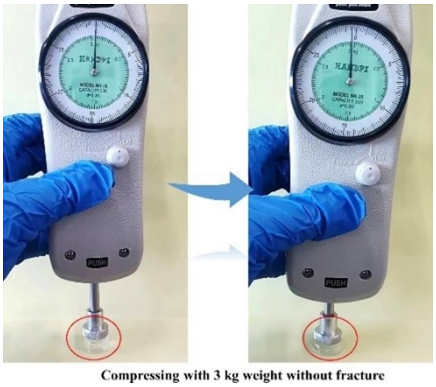

Fig. S14 Loading capacity (3 kg) of the cylindrical C_{18}-PCHA-AAm hydrogel electrolyte.

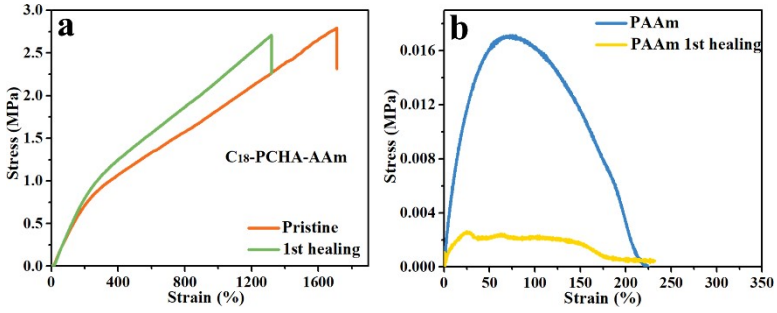

Fig. S15 Tensile strain-stress curves of the original and self-healed (a) C_{18}-PCHA-AAm and (b) PAAm hydrogel electrolytes.

Fig. S16 The thickness of C_{18}-PCHA-AAm hydrogel electrolyte.

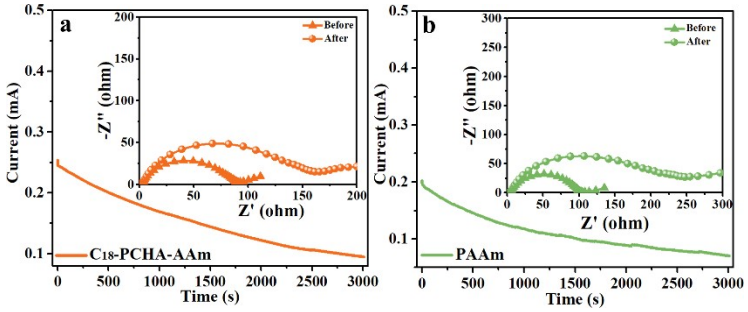

Fig. S17 Chronoamperometry plots of C_{18}-PCHA-AAm and PAAm hydrogel electrolytes (inset: EIS plots before and after polarization).

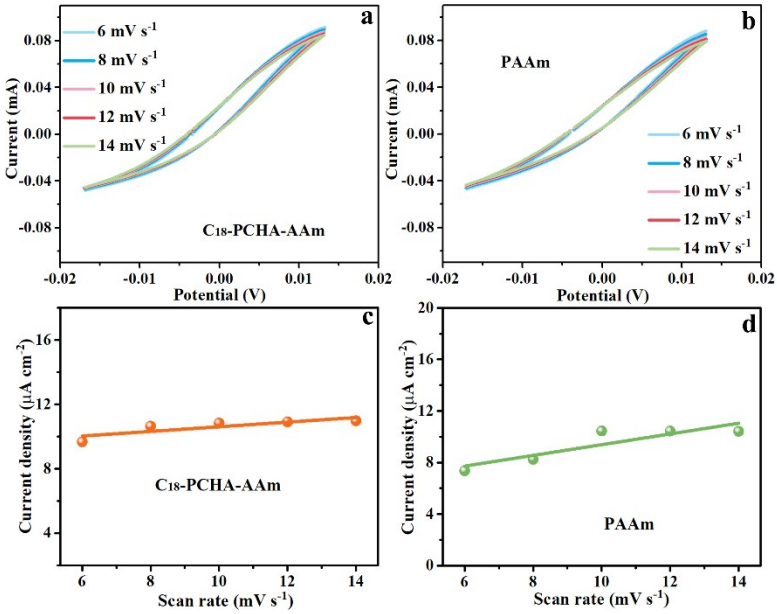

Fig. S18 CV curves of Zn//Zn cells in (a) C_{18}-PCHA-AAm and (b) PAAm hydrogel electrolytes. (c, d) The corresponding calculated double layer capacitance at Zn electrode surface in different electrolytes.

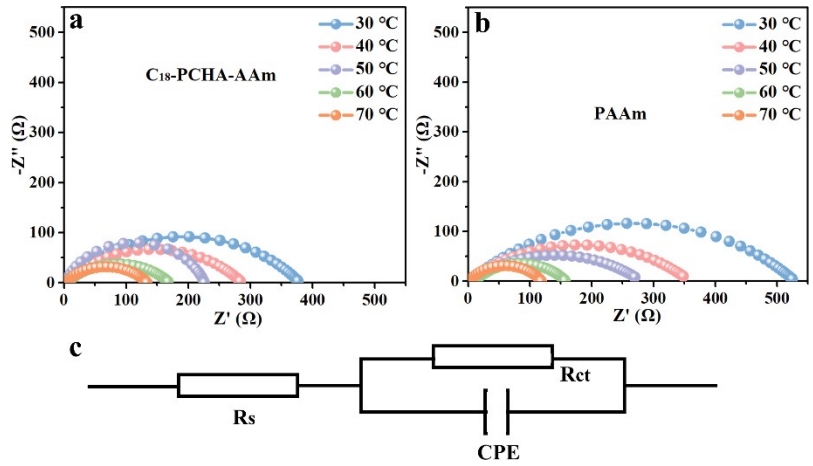

Fig. S19 EIS spectra (Nyquist plots) of Zn//Zn cells at different temperatures in (a) C_{18}-PCHA-AAm and (b) PAAm hydrogel electrolytes. (c) The equivalent circuit.

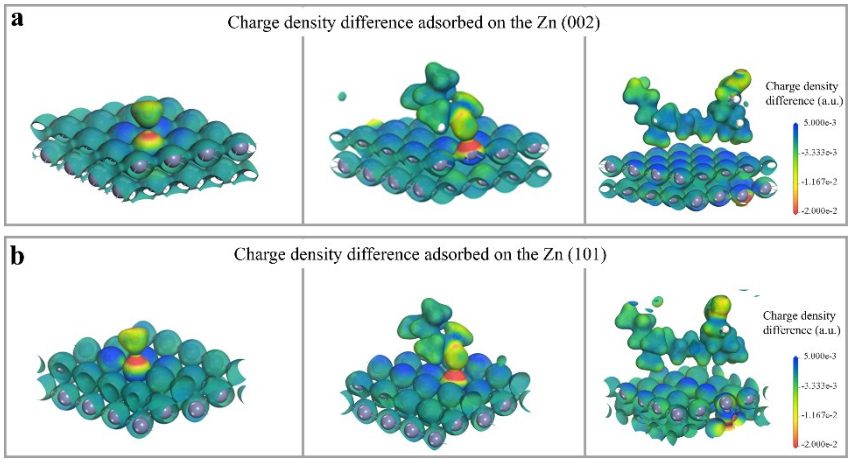

Fig. S20 The charge density difference of H_2O, PAAm and C_{18}-PCHA-AAm adsorbed on the (a) Zn (002) and (b) Zn (101).

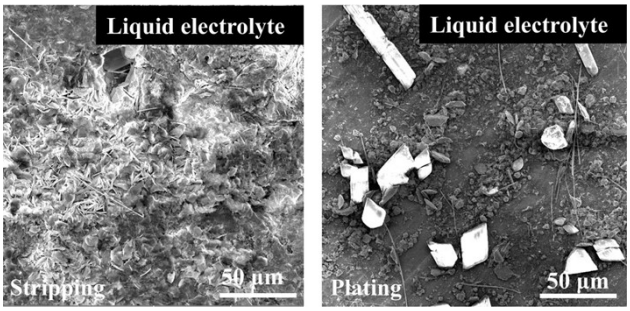

Fig. S21 SEM images of Zn anode with liquid electrolytes at initial stripping states at 1 mA cm^{-2} for 1 h.

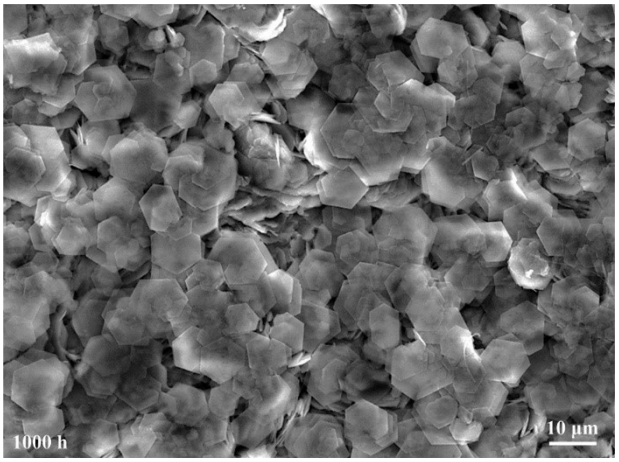

Fig. S22 The SEM images of Zn anodes with C_{18}-PCHA-AAm hydrogel electrolytes after cycling for 1000 h at 2 mA cm^{-2}.

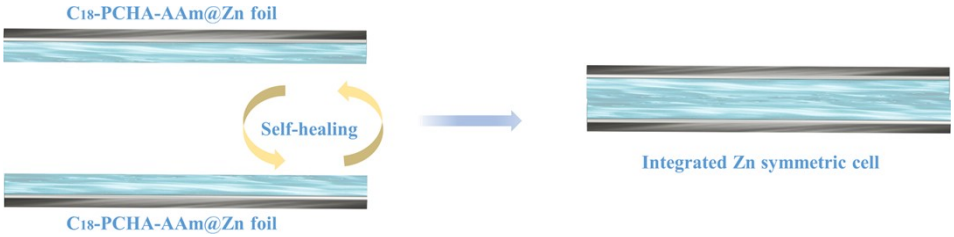

Fig. S23 Illustration of in-situ polymerization Zn/C_{18}-PCHA-AAm/Zn symmetric cell.

As depicted in Fig. S23, although single Zn foil is in-situ fixed with C_{18}-PCHA-AAm hydrogel electrolyte, the self-healing capability in hydrogel electrolyte can integrate them into a whole Zn symmetric cell.

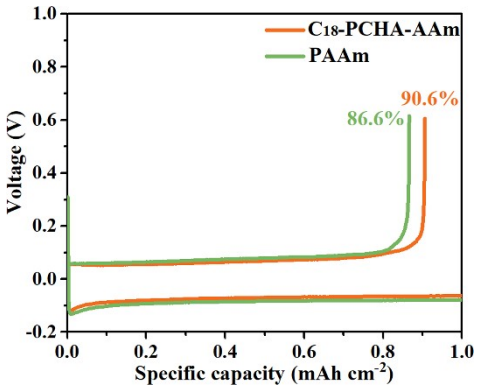

Fig. S24 Voltage profiles of Zn//Cu cells in different hydrogel electrolytes at 1st cycle.

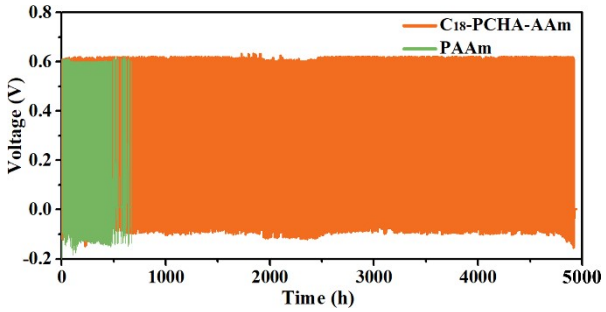

Fig. S25 Voltage profiles of Zn//Cu cells with different hydrogel electrolytes at 1 mA cm^{-2} and 1 mAh cm^{-2}.

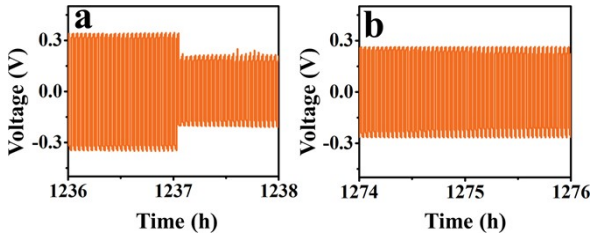

Fig. S26 Enlarged Fig. 6e around (a) 1236 h, (b) 1274 h.

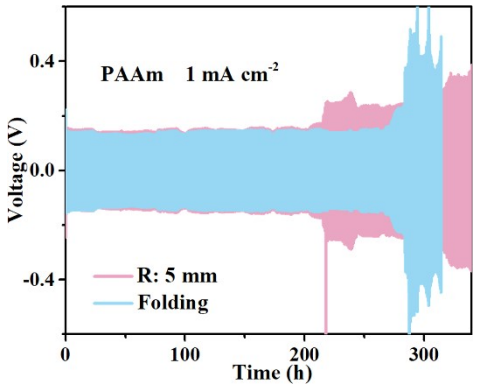

Fig. S27 Voltage-time profiles of Zn symmetric cells with PAAm hydrogel electrolytes under bending with R=5 mm and folding states.

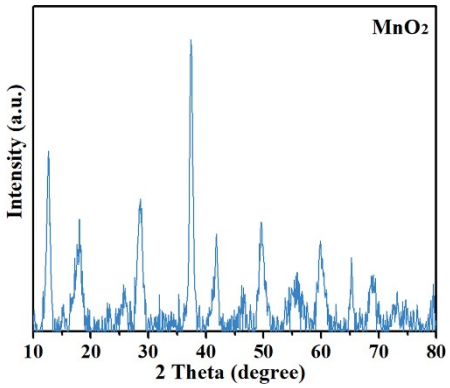

Fig. S28 XRD patterns of MnO_2.

All peaks indicate the crystalline phase of α-MnO_2 (JCPDS NO: 44-0141).

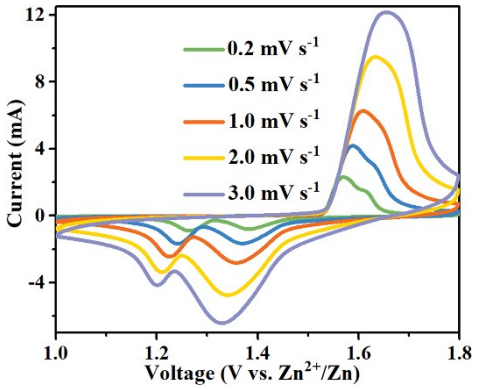

Fig. S29 CV curves of AZIB with C_{18}-PCHA-AAm hydrogel electrolyte at various scan rates.

Table S2. The cycling performance of currently reported hydrogel electrolytes in AZIBs

Hydrogel electrolyte	Cathodes	Cycling stability	Mechanical shock	Ref.
R-ZSO	V_2O_5	1000 cycles, 2C, 72%	Folding, needling, cutting	Angew. Chem. Int. Ed. **2024**, 63, e202318928.
CH/D/Fe	PEDOT-V_2O_5	1000 cycles, 74%, 2.0 A g^{-1}	Bending, folding, rolling	Adv. Funct. Mater. **2024**, 34, 2309048
PCZ-gel	NVO	2000 cycles, 86%, 2 A g^{-1}	Bending, hammering, puncturing	Angew. Chem. Int. Ed. **2023**, 62, e202217833
C-PAMCS	$Cu_xV_2O_5{\cdot}nH_2O$	1000 cycles, 76.8%, 10 A g^{-1}	Bending, twisting	Adv. Mater. **2023**, 35, 2300498
PAGE	PANI	1000 cycles, 3 A g^{-1}; 15 A g^{-1}, 30000 cycles	Bending	Angew. Chem. Int. Ed. **2023**, 62, e202215060
ZA	MnO_2	500 cycles, 2 C	Bending	Adv. Funct. Mater. **2023**, 33, 2300952
SFPAM-Zr	PANI	5000 cycles, 5 A g^{-1}		Energy Environ. Sci., **2023**, 16, 4561
SZHEs	AC	2 A g^{-1}, 50000 cycles, 96.5%	Squeezing, rolling, folding, compressing, punching, cutting, bending, twisting	Energy Environ. Sci., **2023**, 16, 1291
OR-PUU/PAM	MnO_2	2 A g^{-1}, 2000 cycles,	Bending, cutting, healing	Adv. Mater. **2024**, 2311082
C_{18}-PCHA-AAm	MnO_2	3000 cycles, 86%	Bending, cutting, healing	This work

3. Notes and references

1 T. Lu and F. Chen, *J Comput Chem*, 2012, **33**, 580–592.

2 W. Humphrey, A. Dalke and K. Schulten, *Journal of Molecular Graphics*, 1996, **14**, 33–38.